EFFECT OF FOREIGN OBJECT DAMAGE ON THE FATIGUE STRENGTH OF AN XD™ γ-TiAl ALLOY

T.S. Harding[1] and J.W. Jones[2]

[1]Industrial and Manufacturing Engineering and Business Department, Kettering University,
Flint, MI 48504-4898
[2]Department of Materials Science and Engineering, University of Michigan,
Ann Arbor, MI 48109-2136

Introduction

High cycle fatigue has become the leading cause of failure in gas turbine engine blades in recent years [1]. The majority of these failures were associated with surface damage such as foreign object damage (FOD). Therefore, the ability of a material to resist impact damage and the subsequent fatigue propagation of any cracks that may result has become a crucial design consideration. Substantial research has been conducted on the effects of simulated FOD in conventional turbine blade materials where the formation of cracks at the impact site was not a common occurrence [2,3,4]. However, impacts of more brittle materials, such as γ-TiAl, would likely result in the formation of cracks. Steif *et al* [5] have examined the formation of cracks associated with impacts in several TiAl-based alloys. The effects of ballistic impacts on the fatigue behavior of a Ti-48Al-2Nb-2Cr γ-TiAl alloy were examined by Lerch *et al* [6]. Fatigue strength was correlated with a somewhat arbitrary crack length with some success; however, no correlation with the long-crack fatigue threshold was made. The use of a fatigue threshold limit may be necessary for design of turbine blades given the limited fatigue crack growth resistance exhibited by γ-TiAl.

The present study investigates the reduction in elevated temperature fatigue strength of a Ti-46.8Al-2.1Nb-1.1Mn-0.1Si-1.4B alloy caused by simulated foreign object damage. This work is part of a larger effort to support the transition of γ-TiAl to industrially relevant gas turbine engine applications.

Materials and Experimental Procedure

The γ-TiAl alloy examined in the present study had a nominal composition of Ti-46.8Al-2.1Nb-1.1Mn-0.1Si-1.4B (at.%) and is referred to as "47XD." Produced using the XD™ process [7], the alloy was first induction skull melted into ingot form and subsequently vacuum arc remelted and investment cast into 10mm $\times$ 150mm $\times$ 12.5mm plates. The castings were then hot isostatically pressed at 1185°C at 175MPa for 4h. This heat treatment resulted in the near-fully lamellar microstructure shown in Figure 1 with dispersed needle-like TiB_2 precipitates ($\sim$5–10 μm long and $\sim$1μm in diameter). Lamellar colonies were approximately 110μm in diameter. The microstructure consisted of approximately 15.0vol.% α_2 phase, $\sim$1vol.% TiB_2 phase and the remainder in the γ phase. While the α_2 phase was
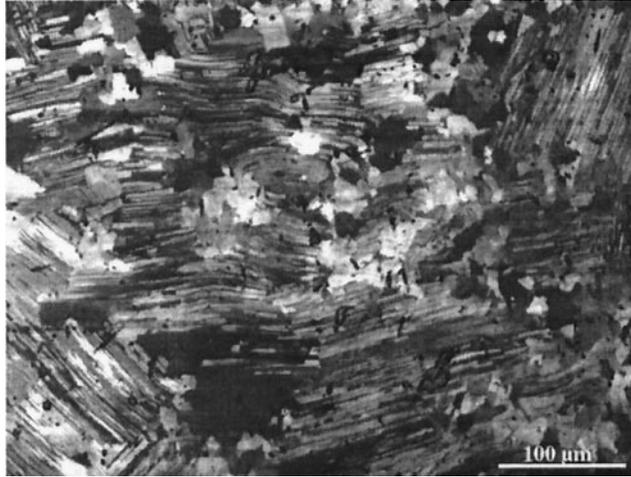
Figure 1. Optical micrograph of the near-fully lamellar Ti-46.8Al-2.1Nb-1.1Mn-0.1Si-1.4B alloy showing 110μm lamellar colonies with smaller equiaxed γ grains within the lamellar colonies.

present primarily as lamellar plates, the γ phase was found both in lamellar colonies as well as small ($\sim16\mu$m) equiaxed gamma grains located within the lamellar colonies.

Fatigue specimens were produced by electro-discharge machining the cast plates into blanks that were then low stress ground to the nominal dimensions shown in Figure 2. The specimen geometry was designed to represent the leading edge of a turbine blade. The chamfered surfaces in the gage section (see inset in Figure 2) were produced by surface grinding. Each specimen was electropolished to a mirror finish in a perchloric solution.

Ballistic impacts were performed using a gas powered barrel to propel 1.6mm steel ball-bearings at the chamfered face of the specimens as shown schematically in Figure 3. The projectiles were fired at the specimens at nominal speeds of 100–250m/s. All impacts were conducted at room temperature under zero load. Figure 3 also indicates the general appearance of the various damage classifications observed following impact. These classifications are used for establishing general damage conditions.
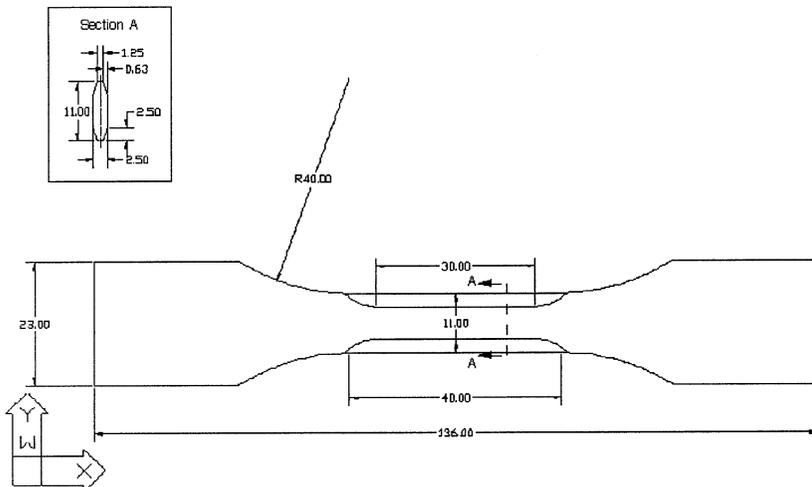

Figure 2. Specimen geometry of blade-like fatigue specimens used for simulated foreign object damage study.

1.59 mm
Ball-bearing

Impact
Velocity

Hertzian-like
Crack
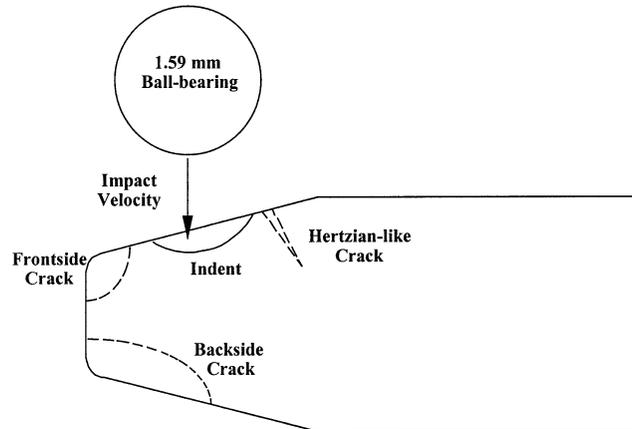
Frontside
Crack

Indent

Backside
Crack

Figure 3. Schematic illustration of the ballistic impact process and the damage introduced in the fatigue specimen. The figure shown is one-half of the cross-sectional view of the gage section.

Fatigue tests were conducted on a closed-loop servohydraulic mechanical testing machine at 600°C in air. Tests were run at a frequency of 20Hz with a load ratio of R = 0.1. Fatigue strength was determined using the step-test method [8] in which the applied stress is steadily increased in a step loading fashion while load ratio is kept constant. In the present study, the maximum cyclic stress was increased by 10MPa every 10^5 cycles until failure. The fatigue strength is defined as the highest stress at which a specimen survived a full 10^5 cycle block without failure. Given the flatness of the stress-lifetime curves of many γ-TiAl alloys [9,10], this measure of fatigue strength is considered to be a reasonable approximation of the endurance limit of the damaged specimens.

Results and Discussion

Impact Damage

Ballistic impacts resulted in cracks of one of three different types, in addition to an impact crater. These categories are described as backside cracks, frontside cracks and Hertzian-like cracks as shown schematically in Figure 3. Backside cracks are believed to form when a bending moment is introduced during the impact that acts about the axis perpendicular to the loading axis and parallel to the specimen's width. Consequently, the high tensile stresses and plastic strain developed on the back face of the specimen lead to crack formation. Cracks of this type are typically the largest, being over 1mm in length on average. Frontside cracks are corner cracks that form at the base of the impact crater, and are typically smaller than backside cracks (100–500µm). These cracks are likely a result of the lack of constraint near the specimen edge of the hoop stresses surrounding the impact crater.

A special variety of crack was observed in one of the impacted specimens referred to as a Hertzian-like crack for its resemblance to the Hertzian cone cracks formed during impact of a brittle material [11]. As shown in the schematic illustration in Figure 3, the Hertzian-like cracks tend to form behind the impact crater and propagate into the depth of the specimen at an angle to the specimen surface, roughly 55° in the case of the 47XD alloy. From the surface, these cracks have a crescent shape. It is believed that the formation of a Hertzian-like crack is a result of the radial stresses surrounding the impact crater exceeding a critical value. Additional research is currently being conducted to further investigate the crack formation mechanism.
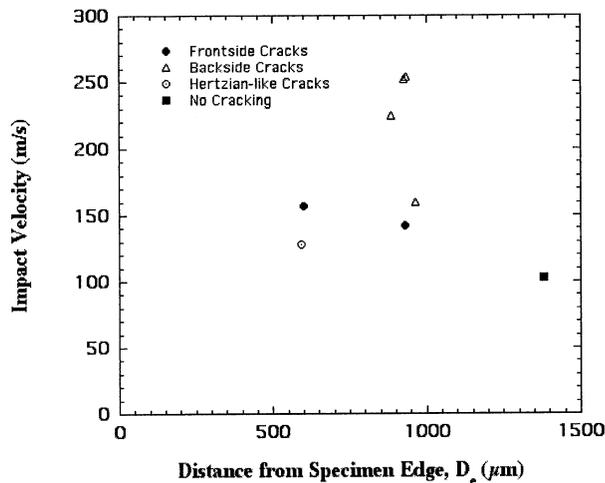
Figure 4. Effect of impact velocity and the location on damage type in the ballistically impacted 47XD alloy.

For the ballistic impacts, the position of the impact site and the impact velocity were chosen to produce a variety of crack sizes and geometries suitable for fracture mechanics analysis. Each specimen was impacted once according to the procedure described above. Specimens were impacted at nominal positions of 500, 1000 and 1500μm from the specimen edge. For each impact damaged specimen, the critical damage type was identified as that which led to fatigue failure as determined from fractography. As Figure 4 shows, at a distance of 1000μm from the specimen edge, the dominant damage type was a backside crack at moderate to high impact velocities. Backside crack size was observed to increase with increasing impact velocity. At low velocities, frontside cracks appear to be the dominant damage type. Closer to the specimen edge, impacts at relatively low velocities resulted in the formation of frontside and Hertzian-like cracks, suggesting that the formation of these sorts of cracks may be highly dependent on impact location. Furthermore, far from the specimen edge and at very low impact velocities, the impact resulted in only the formation of a crater with no signs of cracking at the specimen surface. This suggests that for the specimen geometry and impacting procedure examined here there is a critical combination of impact location and velocity below which no cracking will occur.

Reductions in Fatigue Strength

The reduction in fatigue strength caused by the impact event was examined both in terms of the type of damage, as well as, the size of the critical crack that grew to failure. The reduction in fatigue strength resulting from each damage type is shown in Figure 5. Relative to the fatigue strength of undamaged specimens, Hertzian-like cracks appear to be the least severe form of damage, though only a single specimen failed by this damage type. Frontside cracks appear to cause the next greatest reduction in fatigue strength on average, though there is considerable scatter in the measured results. Finally, backside cracks cause the most significant reduction in fatigue strength.

γ-TiAl alloys have been shown to have limited damage tolerance, particularly at 600°C [12,13]. In order to avoid high cycle fatigue failures in impact damaged γ-TiAl, a design philosophy based on fatigue crack growth thresholds may be necessary. Therefore, the reductions in fatigue strength in the 47XD alloy caused by the damage examined here should be compared with an estimated threshold stress. However, the variation in damage geometry requires that calculated stress intensity for each flaw be compared with the threshold stress intensity rather than directly comparing stresses. The size and
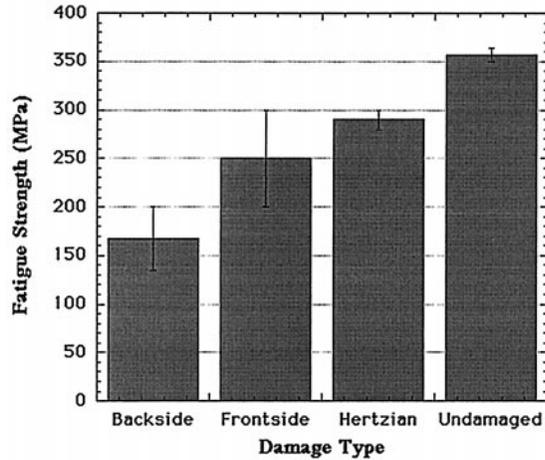
Figure 5. Reduction in fatigue strength for ballistically impacted 47XD as a function of damage type. The fatigue strength of undamaged material is shown for comparison.

shape of the critical flaw were determined from both optical and electron microscopy. For most cases, the cracks could be defined as quarter elliptical corner cracks for which a Raju-Newman solution of the stress intensity was used [14]. For Hertzian-like cracks, however, the stress intensity could not be easily defined, as the crack is primarily situated parallel to the loading axis. Therefore, the initial flaw size was defined as a region of flat crack growth perpendicular to the loading axis and situated at the apex of the primary Hertzian-like crack and the specimen surface.

To obtain the threshold stress intensity, fatigue crack growth rate tests were conducted at 600°C. The results of this experiment are shown in Figure 6a). The calculated stress intensities of the impact damage are in essence threshold stress intensities since the fatigue strength was used in the Raju-Newman calculation. Therefore, direct comparison can be made between the long-crack fatigue thresholds in Figure 6a) and the calculated stress intensities. This is accomplished using the modified Kitagawa-like plot shown in Figure 6b). Good correlation between the long-crack thresholds (ΔK_{TH} and
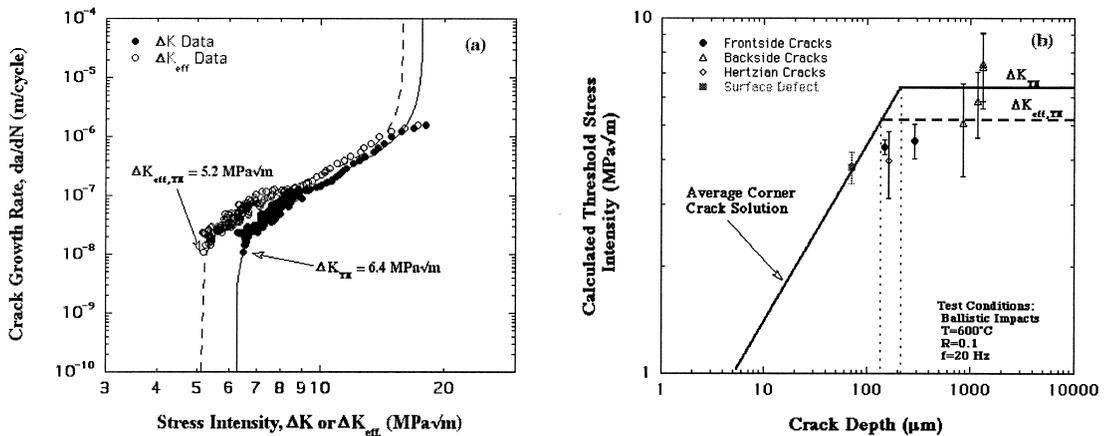

Figure 6. a) Results of fatigue crack growth rate tests on the 47XD alloy, b) Calculated threshold stress intensity of impact damage as a function of crack depth and damage type. The sloped line represents the endurance limit of undamaged material. Error bars relate to the variation in stress intensity along the crack front.

$\Delta K_{eff,TH}$) and calculated stress intensity is observed for large, backside cracks. However, for cracks less than approximately $400\mu m$ in size, the calculated stress intensity is less than both the long-crack threshold stress intensity and the endurance limit. This suggests that for cracks less than approximately 5 times the average lamellar colony size the long-crack fatigue threshold stress intensity may be inappropriate for estimating the fatigue strength. Instead, a small-crack threshold may be needed.

Conclusions

Based on an experimental study of the reduction in fatigue strength caused by simulated foreign object damage in a near-fully lamellar Ti-46.8Al-2.1Nb-1.1Mn-0.1Si-1.4B alloy damaged by the method examined here, the following conclusions can be made:

1. Damage resulting from the types of impacts used here was classified into one of three categories: backside, frontside or Hertzian-like cracks. Impact velocity and location were found to play an important role in both the type and severity of damage produced.
2. The reduction in fatigue strength caused by the impact damage could be roughly correlated with the type of damage produced from the impact.
3. The calculated threshold stress intensities of large backside cracks agreed well with the long-crack fatigue thresholds (ΔK_{TH} and $\Delta K_{eff,TH}$). However, it appears that a small crack threshold is needed to estimate the fatigue strengths of specimens with cracks less than five lamellar colonies in length.

Acknowledgments

References

1. B. A. Cowles, Int. J. Fract. 80, 147 (1996).
2. O. Roder, J. O. Peters, A. W. Thompson, and R. O. Ritchie, in Proceedings of the 4th National Turbine Engine High Cycle Fatigue Conference, 1999, University Technology Corp., Dayton, OH, in press.
3. S. J. Hudak, C. G. Chell, T. S. Rennick, R. C. McClung, and D. L. Davidson, in Proceedings of the 4th National Turbine Engine High Cycle Fatigue Conference, 1999, University Technology Corp., Dayton, OH, in press.
4. T. Nicholas, J. P. Barber, and R. S. Bertke, Exp. Mech. 20(10), 357 (1980).
5. P. S. Steif, M. P. Rubal, G. T. Gray III, and J. M. Pereira, J. Mech. Phys. Solids. 46, 269 (1998).
6. B. A. Lerch, S. L. Draper, G. Y. Baaklini, and J. M. Pereira, in HITEMP Review 1999: Advanced High Temperature Engine Materials Technology Project, 1999 NASA CP 1999–208915/vol. 2, paper 30.
7. K. S. Kumar, J. A. S. Green, D. E. Larsen Jr., and L. D. Kramer, Adv. Mater. Processes. 147(4), 35 (1995).
8. J. A. Collins, Failure of Materials in Mechanical Design, p. 379, John Wiley and Sons, New York (1993).
9. J. Kumpfert, Y-W. Kim, and D. M. Dimiduk, Mater. Sci. Eng. A. 192/193, 465 (1995).
10. E. J. Dolley, N. E. Ashbaugh, and B. D. Worth, in Fatigue '96: Proceedings of the 6th International Fatigue Congress, vol. III, ed. Lütjering and Nowack, p. 1755, Elsevier Ltd., Oxford (1996).
11. T. R. Wilshaw, J. Appl. Phys. D. 4, 1567 (1971).
12. S. J. Balsone, J. M. Larsen, D. C. Maxwell, and J. W. Jones, Mater. Sci. Eng. A. 192/193, 457 (1995).
13. A. H. Rosenberger, B. D. Worth, and J. M. Larsen, in Structural Intermetallics, ed. Nathal et al., p. 555, TMS, Warrendale, PA (1997).
14. J. C. Newman Jr. and I. S. Raju, Fracture Mechanics, ASTM STP 791, ed. Lewis and Sines, p. I-238, American Society for Testing Materials, Philadelphia (1981).